DOI: 10.1002/adma.200501975

Silicon Onion-Layer Nanostructures Arranged in Three Dimensions**

By *Alvaro Blanco* and *Cefe López**

Complex material structures are inherently interesting to the curious scientific mind because of the challenge of achieving an in-depth understanding of them. Usually complex order and disordered structures are studied using very different approaches because the tools used to model and predict their properties necessarily need to be dissimilar. Periodicity greatly simplifies their understanding and adds interesting new properties. And, when small length scales are entered, new issues arise, such as quantum confinement, transition into effective media, gaps in their electronic and optical spectra, and novel mechanical and thermal properties.

Realization with actual materials such as silicon provides a strong link with technological platforms such as microelectronics. Besides, the development of semiconductors structured in several ways in the search for novel optical and electronic properties has generated a number of strategies in the methods employed that enrich several areas of materials science, with applications in photonic crystals,[1,2] sensors,[3] micro- and nano-electromechanical devices (MEMs and NEMs, respectively),[4] and solar cells, among others. Self-assembly,[5] combined with filling, etching, backfilling, and other materials-processing techniques (often called templating), offers plenty of new, low-cost possibilities. This approach has proved capable of producing high-quality, large-scale 3D macroporous silicon photonic structures[6] with a full photonic bandgap[7] by templating on artificial opals using chemical vapor deposition (CVD). Combining silicon and germanium CVD it is possible to make the structure more complex and engineer its optical response.[8]

The mentioned CVD process is carried out at around 350–400 °C, which limits the template materials that can be used, silica being most usually employed. However, silica artificial opals, especially in thin-film form,[9] present a number of issues. First, sizes with acceptable monodispersity are limited to 200–500 nm diameter for conventional Stöber synthesis. In order to increase this range, a subsequent regrowth process is needed,[10,11] which limits the beads' quality and slows the fabrication. Second, arranging silica spheres of about a micrometer is a very difficult task and possible in only a very narrow set of experimental parameters.[12] In general, thin artificial opals are more easily produced when polymer beads (poly(methylmethacrylate) (PMMA) or polystyrene (PS)) are used, and their optical quality is far superior. Nevertheless, when high temperatures (above 100 °C) are required, these polymer artificial opals become useless as templates.

Current procedures have dealt with this problem by proposing a previous infiltration of the air cavities with silica at room temperature, which produces resilient silica templates for further processing. In the case of direct laser writing (DLW) in polymer templates,[13] complete silica infiltration by CVD and further etching of the polymer has been recently proposed.[14] In PS artificial opals, a sol-gel process has been used to infiltrate the opal voids with silica, which allows silicon to be grown on the inner surface of the silica inverse opals (MISO technique).[15] However, sol-gel silica infiltration leads to complete infiltration, with a poor or no degree of control.

In this communication we propose a different strategy that allows not only silicon infiltration in polymer 3D templates, but also finer tuning of their photonic crystal properties. By means of silica CVD it is possible to finely control the degree of infiltration in polymer opals, which can be used to generate a novel topology consisting of an interconnected double network of concentric layers of silicon. These 3D macroporous silicon structures may be of importance due to their versatile photonic properties tailored through design.

PS and PMMA spheres of different sizes (ranging from 300 to 1100 nm) were arranged by the vertical deposition method to form thin artificial opals, which were used as templates for further processing. Using a polymer opal as a templates, (Fig. 1a) we grew a silica layer around the spheres by room temperature CVD (Fig. 1b) with the desired thickness and, therefore, to the desired degree of infiltration. After this treatment, the polymer was removed by calcination of the composites, leaving a 3D porous structure of silica shells (Fig. 1c), which can then be used for silicon infiltration at higher temperatures. Here, owing to silica partial infiltration, silicon can grow on both the inner and the outer surfaces of silica layers. At this stage, all that is needed is an entry point opened in the silica for the disilane to reach the whole interior of the structure. This may be provided by a naturally occurring crack or can be prepared by, for instance, selective reactive ion etching or other means.[16] The internal spherical air cavities are connected by circular windows of diameter d (Fig. 1d), which originate from the contact points between spheres. The size of these windows may vary depending on

[*] Prof. C. López, Dr. A. Blanco
Instituto de Cienca de Materiales de Madrid (CSIC) and
Unidad Asociada CSIC-UVigo
C/ Sor Juana Inés de la Cruz 3, 28049 Madrid (Spain)
E-mail: cefe@icmm.csic.es

[**] This work has been partially financed by the Comunidad Autónoma de Madrid (Project GR/MAT/0430/2004), the Spanish MEC through project MAT-2003-01237, and the EU NoE PhOREMOST contract 511616.

ADVANCED MATERIALS

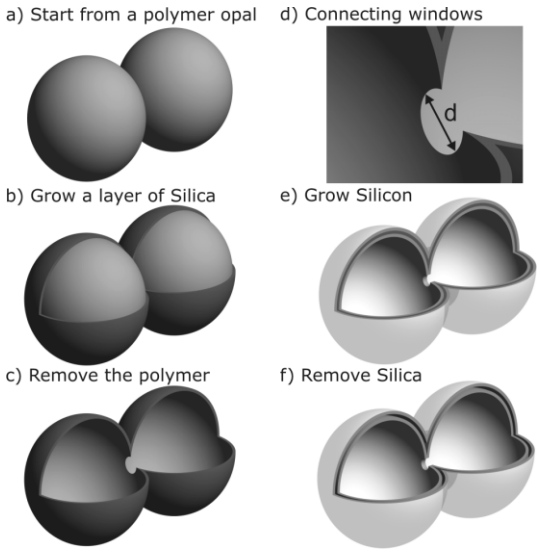

Figure 1. Fabrication process: a) Start with a polymer opal. b) A silica layer is grown by CVD around spheres. c) Removal of polymer by calcination. d) At the contact points between spheres windows of diameter *d* open, connecting spherical cavities. e) Silicon is grown by CVD and the internal silica layer is removed by etching in HF. The result is a double silicon network formed by concentric spherical layers (f).

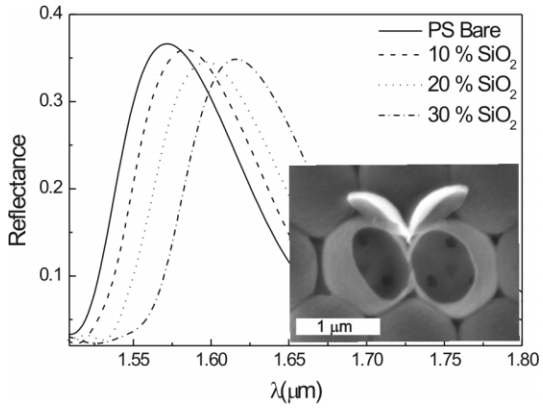

Figure 2. Silica infiltration process. Spectra show how the Bragg peak for a bare opal (solid line) shifts from around 1.56 to 1.62 μm due to refractive index change. The curves correspond to silica layer thicknesses of 5, 9, and 14 nm. Inset: Scanning electron microscopy (SEM) image of the silica shells (two of which are cracked) after polymer calcination.

several factors (such as the infiltrated material and template wettability) and for CVD silica is usually about 10 % of the sphere diameter. These connecting windows make silicon growth possible on the inner surface to a layer thickness of *d*/2, the point at which the windows close, preventing further conformal growth. Here it is assumed that silicon will grow equally outside and inside the silica shell, producing two layers of the same thickness. The final structure consists of onion-like multilayered silicon/silica/silicon spherical strata enclosing air cavities. Their thicknesses can be easily controlled through experimental parameters (Fig. 1e). Furthermore, the silica can be selectively etched with dilute HF, producing a final all-silicon structure consisting of concentric air-separated spherical shells ordered in three dimensions (Fig. 1f). The power of the method lies in the fact that the geometrical magnitudes (sphere size, layer thicknesses, etc.) of structures of this kind can be easily and independently controlled by experimental parameters, which will finally determine, for example, their photonic response. Even the final inner silicon layer thickness can be controlled by adjusting the initial filling fraction of the polymer opal, thus modifying the connecting window size *d* (which can be done by sintering).[17]

Figure 2 illustrates the progress of the silica infiltration process, showing four reflectance spectra in a 705 nm PS sphere template. The peak, associated with the first pseudogap opening at point L of the Brillouin zone, shifts as we increase the silica-layer thickness owing to the increase in average refractive index. Under the conditions used in our case, three consecutive silica CVD cycles led to 10, 20, and 30 % of the pore volume being infiltrated, which corresponds to thicknesses of 5, 9, and 14 nm, respectively, indicative of the nanometer-level control. Scanning electron microscopy (SEM) inspection at this stage demonstrated that we were able to grow thin silica layers that cover the PS spheres and preserve the original opal symmetry after the polymer beads have been removed by calcination (inset to Fig. 2). When the silica shells crack, the empty interior of the spheres is visible. The windows connecting spherical silica cages (whose size sets the limit to further inner silicon growth) can also be seen. It is important to point out that this first silica infiltration step is critical in the whole fabrication process as many of the properties of the final structure will depend on it. In addition, structures like the one shown in Figure 2b can consist of 97 % air and have an average refractive index as low as 1.03 with a controlled overall thickness (from sub- micrometer to some micrometers, given by the original thin artificial opal) and can be seen as 3D ordered silica aerogels.

Once the silica scaffold has been prepared from the initial polymer structure, silicon CVD can be performed without problem. Again, silicon growth from the gas phase allows smooth coatings with accurate thickness control and in a conformal way around silica shells. Figure 3 shows SEM images of different silica samples infiltrated with silicon. The infiltration process does not depend on the number of layers, as can be observed in Figure 3, where 1–2 (Fig. 3a), 5–6 (Fig. 3b), or tens of efficiently prepared layers (Fig. 3c) can be seen. Notice how silicon reproduces the original silica shell skeleton with extreme faithfulness after CVD. It is important to point out that the grown silicon is amorphous (a-Si). Nevertheless, it can be crystallized by annealing at 600 °C for several hours if required. Additionally, it would be possible to grow a new silica layer at this point of the fabrication process. Again it would grow both on the inside and outside surfaces of the silicon layers. This process can be repeated while connecting windows remain open: outer shells can grow conformally to up to 86 % of the initial opal pore volume (layer thickness around 16 % of the sphere radius for a perfect face-centered cubic

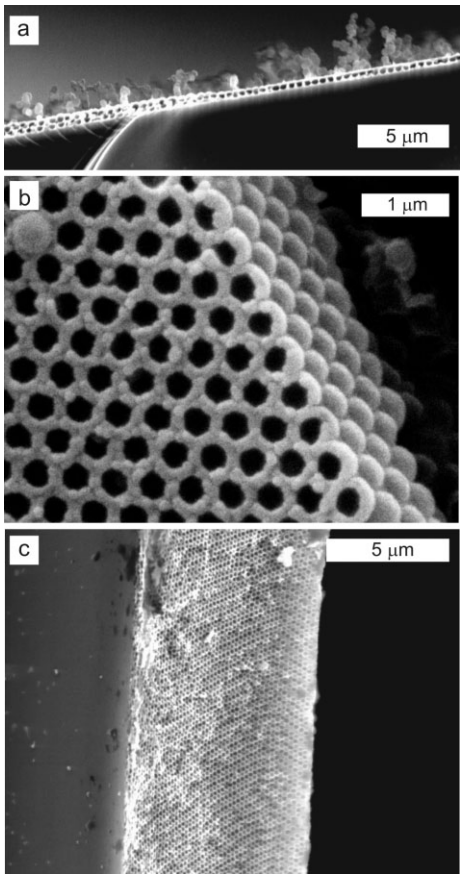

Figure 3. SEM images from cleft edges of silicon grown on silica shell opals. a) One monolayer and transition to two monolayers. b) Five-to-six monolayers. c) Thick samples with tens of monolayers can be easily prepared by this method preserving the initial fcc structure of the initial polymer opals.

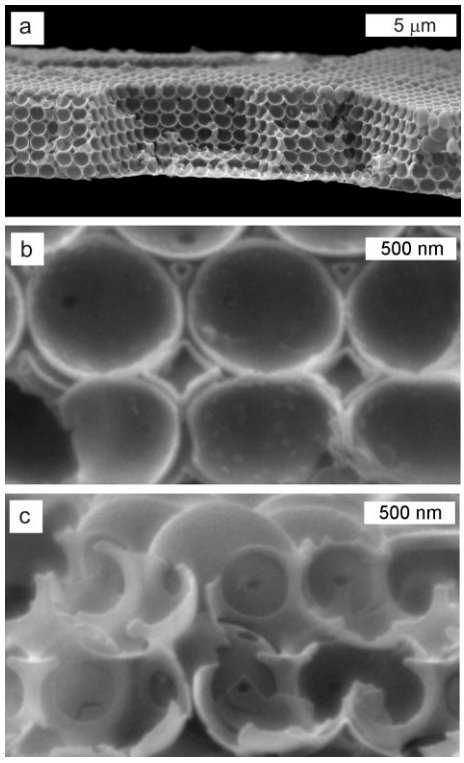

Figure 4. SEM images of silicon–air–silicon structures made from 1100 nm PS spheres. a) Cleft edge of the sample showing six monolayers. b) Detail of the structure in which silicon/air/silicon interfaces can be seen. The air gap can be controlled through the initial silica layer. c) Detail of the silicon onion-layer structures formed by concentric open shells revealed by cracking the shells.

(fcc) structure) and inner layers can grow up to a thickness of $d/2$. Up to this point a superstructure is produced consisting of onion-like silicon/silica/silicon layered shells surrounding empty pores arranged in fcc symmetry. This type of structure holds promise since amorphous Si/SiO_2 nanometric superlattices have shown light emission due to quantum confinement.[18] This property, combined with the photonic crystal nature of the 3D superstructure, might be exploited in terms of spontaneous emission inhibition[19] and, eventually, lasing, which would add a richer functionality.

The next step, removing the internal silica layer, will produce a nanometric spherical air gap separating two macroporous silicon networks. These two silicon networks are both attached to the substrate on which the opal is grown, which gives the necessary mechanical stability to the structure. Figure 4 shows SEM images of an opal (sphere diameter $D = 1100$ nm) after etching of the silica layer. At this final stage it is possible to observe the internal nanostructured shells enclosing the cavities once occupied by the polymer spheres. Figure 4a shows a cleft edge of this sample, where around six monolayers can be seen. A closer look at the structure (Fig. 4b) reveals the multilayered spherical shells. Outer and inner silicon layers separated by an air gap can be easily seen. It is also possible to estimate these layers' thicknesses as ca. 30 nm. The actual inner and outer silicon layer thicknesses are almost the same, as we assumed. Figure 4c shows a higher magnification image of a cracked region of a double-shell inverse opal. The crack is very irregular, which complicates its interpretation. This is caused by the fact that the two silicon shells crack independently, revealing different details of the inner and outer shells. In particular, the inner shells sometimes appear through the (larger) windows in the outer ones. Notice that some of the outer shells appear empty as a consequence of the removal of their interior. In support of this interpretation and to ease the correct visualization of this complex structure, we provide a computer-generated 3D model in Figure 5. In the upper picture, a double silicon network inverted structure is modeled, which has been cut to show (111) (center triangle) and (100) facets. The bevel in the upper picture corresponds to a (110) cleavage made to expose the concentric spherical cavities, where the inner shells can readily be seen. In the bottom picture of Figure 5, a detail of the structures is shown to realistically reproduce what is seen in Figure 4b. Here, one can see the line where the (111) and (100) planes meet. Upon careful inspection one can observe the accurate match between model and reality.

ADVANCED MATERIALS

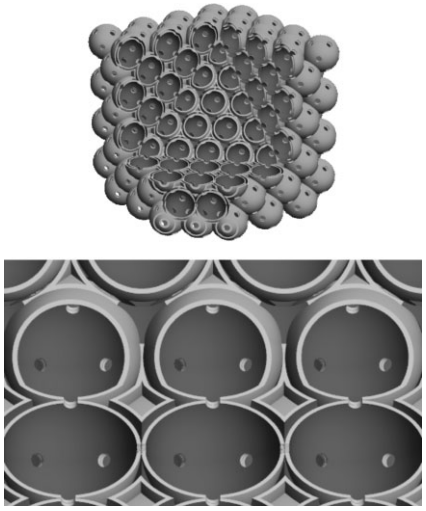

Figure 5. Computer-modeled structures showing the interpenetrated silicon double-shell network. By using cylinders to simulate connecting windows and planes to show inner surfaces it is possible to reveal the onion-like heterostructures like the ones appearing in Figure 4.

The optical properties of the structures, which we used here as a tool to monitor the fabrication process, are shown to be extremely sensitive to changes in both morphology and composition (refractive index). This fact allows a very accurate estimate of the materials content in the sample, provided the refractive index is known. In Figure 6 we have summarized this process in terms of the optical (photonic) response of the structures by plotting specular reflectance and transmittance versus wavelength. In Figure 6a, reflectance (solid line) and transmittance (dashed line) from a PS bare opal (698 nm sphere diameter) are shown. The reflectance spectrum features a first-order pseudogap (Bragg peak) around 1620 nm and sharp high-energy peaks along with Fabry–Perot oscillations. A sharp drop in the transmittance near $\lambda \sim a$ (a being the lattice parameter, $2^{1/2} D$) can be seen, caused by diffractive phenomena.[20] After silica CVD infiltration of 25 % of the pore volume (silica layer around 11 nm thick) the reflectance peak shifts some 40 nm (Fig. 6b). After calcination the polymer is removed and the Bragg peak shifts back to higher energies due to the decrease in the average refractive index (Fig. 6c). Here the peak intensity is really weak because the system behaves as a homogeneous medium with an average refractive index very close to unity (estimated to be $n_{av} \sim 1.03$) due to a very low filling fraction (around 5 % silica, 95 % air). At this stage, the sample can hardly be seen by the naked eye, which is consistent with its transmittance being very close to unity (Fig. 6c). However, after silicon infiltration this peak shifts again, this time to lower energies, owing to higher average refractive index, and recovers intensity (Fig. 6d), owing to a higher dielectric contrast. In addition, high energy features become more intense, developing a much richer structure. This is a signature of broadening of the gaps and flattening of the bands in the spectral range where full photonic bandgaps will eventually appear for structures of this kind. When silica

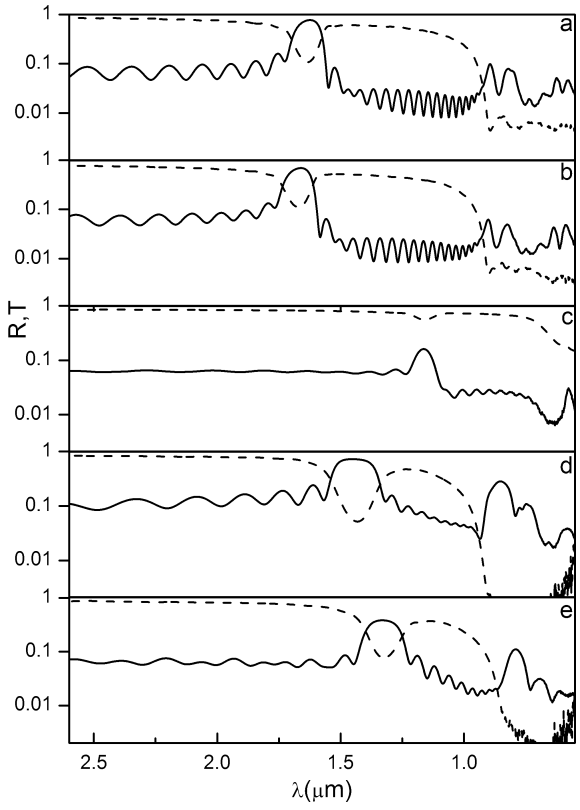

Figure 6. Specular reflectance (solid lines) and transmittance (dashed lines) measurements taken at each stage of the fabrication process for a sample with lattice constant $a = 0.98$ μm. a) PS bare opal. b) Silica-infiltrated PS opal. c) Silica inverse opal resulting after calcination. d) Silicon/silica/silicon structure after CVD silicon infiltration. e) Silicon/air/silicon structures after silica etching with HF.

is dissolved, the Bragg peak slightly shifts to higher energies (Fig. 6e), owing to the lower index of the air gap. Depending on the initial silica layer thickness this final shift in the photonic response can be finely controlled, if required.

Owing to the fact that the first step of the process, the silica infiltration, is done at room temperature, the present strategy can be applied to any kind of polymer. In particular, as mentioned in the introduction, it could be applied to photosensitive resins, extensively used in microelectronics as well as in direct laser writing[21] and 3D holographic lithography.[22] The two latter techniques have been shown to be very promising for the fabrication of 3D photonic crystal templates.

In summary, this communication describes a method to infiltrate silicon in polymeric self-assembled microstructures. By means of combined silica and silicon CVD it is possible to build up multilayered structures arranged in 3D with photonic crystal optical response. These structures are very open and can host other materials with additional functionalities. Bearing in mind the undeniable advantages of polymer opals (and other polymeric structures) in terms of quality, ease of production, and available range, the method outlined in this communication constitutes a great step forward in the fabrication of photonic crystals. Novel topologies, such as silicon con-

centric layers surrounding spherical cavities, are created with this fabrication process, which might prove useful in a wide range of fields.

Experimental

PS and PMMA spheres ($D < 1$ μm) were synthesized by surfactant-free emulsion similar to that reported in the literature [23]. PS spheres with $D > 1$ μm) were acquired from Duke Scientific Corporation with a nominal polydispersity lower than 3 %. Thin film opals were prepared by the vertical deposition method [9].

Silica infiltration was done by room temperature CVD in a home-made reactor as explained elsewhere [24] following a method developed by Míguez et al. [25], which allows the silica-layer thickness to be controlled with nanometer precision via flow rates or reaction times. When the desired silica shell thickness was achieved, samples were calcined in air at 450 °C for 3 h with an initial ramp of 1 °C min^{-1}, to avoid violent evaporation of the polymer.

Silicon CVD was performed at 360 °C at around 150 Torr (1 Torr ≈ 133 Pa) using disilane as precursor with a precision of a few nanometers. The fabrication process was monitored by optical characterization, and the morphology checked by SEM.

Silica was dissolved in 1 wt % dilute HF solution.

Optical transmission and specular reflectance were taken after each fabrication stage to monitor the process, taking advantage of the fact that optical response is very sensitive to changes in both morphology and refractive index of the structures. Optical spectra were taken with a Fourier transform infrared spectrometer IFS 66/S from Bruker, with an optical microscope attached.

Received: September 16, 2005
Final version: February 6, 2006
Published online: ■

Note added in proof:
Gratson et al.[26] and Tétrault et al.[27] have independently realized similar procedures for 3D polymeric structures.

[1] E. Yablonovitch, *Phys. Rev. Lett.* **1987**, *58*, 2059.
[2] S. John, *Phys. Rev. Lett.* **1987**, *58*, 2486.
[3] V. S. Y. Lin, K. Motesharei, K. P. S. Dancil, M. J. Sailor, M. R. Ghadiri, *Science* **1997**, *278*, 840.
[4] W. Lang, *Mater. Sci. Eng. Rep.* **1996**, *17*, 1.
[5] For a recent review see C. López, *Adv. Mater.* **2003**, *15*, 1679.
[6] A. Blanco, E. Chomski, S. Grabtchak, M. Ibisate, S. John, S. W. Leonard, C. López, F. Meseguer, H. Míguez, J. P. Mondia, G. A. Ozin, O. Toader, H. M. van Driel, *Nature* **2000**, *405*, 437.
[7] E. Palacios-Lidón, A. Blanco, M. Ibisate, F. Meseguer, C. López, J. Sánchez-Dehesa, *Appl. Phys. Lett.* **2002**, *81*, 4925.
[8] F. García-Santamaría, M. Ibisate, I. Rodriguez, F. Meseguer, C. López, *Adv. Mater.* **2003**, *15*, 788.
[9] P. Jiang, J. F. Bertone, K. S. Hwang, V. L. Colvin, *Chem. Mater.* **1999**, *11*, 2132.
[10] G. H. Bogush, M. A. Tracy, C. F. Zukoski, *J. Non-Cryst. Solids* **1988**, *104*, 95.
[11] H. Giesche, *J. Eur. Ceram. Soc.* **1994**, *14*, 205.
[12] S. Wong, V. Kitaev, G. A. Ozin, *J. Am. Chem. Soc.* **2003**, *125*, 15 589.
[13] S. Kawata, H. B. Sun, T. Tanaka, K. Takada, *Nature* **2001**, *412*, 697.
[14] A. Blanco, K. Busch, M. Deubel, C. Enkrich, G. von Freymann, M. Hermatschweiler, W. Koch, S. Linden, D. C. Meisel, M. Wegener, in *Photonic Crystals: Advances in Design, Fabrication, and Characterization* (Eds: K. Busch, S. Lölkes, R. B. Wehrspohn, H. Föl), Wiley-VCH, Weinheim, Germany **2004**, Ch. 8.
[15] H. Míguez, N. Tetreault, S. M. Yang, V. Kitaev, G. A. Ozin, *Adv. Mater.* **2003**, *15*, 597.
[16] Y. A. Vlasov, X. Z. Bo, J. C. Sturm, D. J. Norris, *Nature* **2001**, *414*, 289.
[17] H. Míguez, F. Meseguer, C. López, A. Blanco, J. S. Moya, J. Requena, A. Mifsud, V. Fornes, *Adv. Mater.* **1998**, *10*, 480.
[18] Z. H. Lu, D. J. Lockwood, J. M. Baribeau, *Nature* **1995**, *378*, 258.
[19] P. Lodahl, A. F. van Driel, I. S. Nikolaev, A. Irman, K. Overgaag, D. L. Vanmaekelbergh, W. L. Vos, *Nature* **2004**, *430*, 654.
[20] F. García-Santamaría, J. F. Galisteo-López, P. V. Braun, C. López, *Phys. Rev. B* **2005**, *71*, 195 112.
[21] M. Deubel, G. von Freymann, M. Wegener, S. Pereira, K. Busch, C. M. Soukoulis, *Nat. Mater.* **2004**, *3*, 444.
[22] M. Campbell, D. N. Sharp, M. T. Harrison, R. G. Denning, A. J. Turberfield, *Nature* **2000**, *404*, 53.
[23] J. W. Goodwin, J. Hearn, C. C. Ho, R. H. Ottewill, *Colloid Polym. Sci.* **1974**, *252*, 464.
[24] E. Palacios-Lidón, J. F. Galisteo-López, B. H. Juárez, C. López, *Adv. Mater.* **2004**, *16*, 341.
[25] H. Míguez, N. Tetreault, B. Hatton, S. M. Yang, D. Perovic, G. A. Ozin, *Chem. Commun.* **2002**, 2736.
[26] G. M. Gratson, F. García-Santamaría, V. Lousse, M. Xu, S. Fan, J. A. Lewis, P. V. Braun, *Adv. Mater.* **2006**, *18*, 461.
[27] N. Tétreault, G. von Freymann, M. Deubel, M. Hermatschweiler, F. Pérez-Willard, S. John, M. Wegener, G. A. Ozin, *Adv. Mater.* **2006**, *18*, 457.

COMMUNICATIONS

Photonic Crystals

Silicon concentric layers enclosing spherical air cavities is one of the novel topologies created by the method of infiltrating silicon into polymeric self-assembled microstructures. It is shown that by combining silica and silicon CVD it is possible to build up 3D arrangements of multilayered structures (see figure) with a photonic crystal optical response.